Study of the low cyclic behaviour of the IRIS alloy at high temperature

Soumaya Naanani, Muriel Hantcherli, Anis Hor, Catherine Mabru, Jean-Philippe Monchoux, Alain Couret

Study of the low cyclic behaviour of the IRIS alloy at high temperature

Soumaya NAANANI [1,2,*], *Muriel HANTCHERLI*[1], *Anis HOR* [2], *Catherine MABRU* [2], *Jean-Philippe MONCHOUX* [1] and *Alain COURET* [1]

[1] *CEMES, Université de Toulouse, CNRS, 29 rue Jeanne Marvig, 31055 Toulouse, France*
[2] *ICA, Université de Toulouse, CNRS, ISAE-SUPAERO, 10 avenue Edouard Belin - BP 54032 - 31055 Toulouse, France*

Abstract. This paper presents experimental results on low cycle fatigue (LCF) behaviour at high temperatures of the IRIS alloy (Ti-Al_{48}-W_2-$B_{0.08}$, at. %) densified by Spark Plasma Sintering (SPS). Cyclic stability is noticed, whatever the temperature and the total strain amplitude. Fracture occurs by mixed interlamellar and translamellar modes. Transmission electron microscopy (TEM) observations reveal that deformation is mainly due to ordinary dislocations and twins, and slip and cross-slip mechanisms have been clearly evidenced, without significant contribution of climb at 800°C. It has also been established that dislocation density depends on fatigue life time rather than on stress amplitude.

1 Introduction

Extensive investigations on the mechanical properties and processes have allowed commercial implementation of TiAl alloys in aerospace and automotive engines. Their main attractive properties are low density (4g/cm^3) and high strength at high temperature. They are used for instance in low pressure turbine blades of the new generation of aircraft engines, such as the GEnX by General Electric and the LEAP by Snecma-Safran, and in turbine wheels of new generations of turbochargers.
Giving these applications at elevated temperatures, the material is subjected to mechanical and thermal regimes, which generates a large amount of plastic deformation. Low cycle fatigue tests are then used to evaluate the lifetime of TiAl-based alloys, simulating service conditions. Fatigue properties of this class of materials were regularly studied since the pioneering work of Sastry and Lipsitt [1]. Most of these efforts were devoted to binary Ti–Al alloys [3-4] and later to alloys with Nb [5–8].
In this context, IRIS TiAl alloy (Ti-Al_{48}-W_2-$B_{0.08}$ at%) has been developed [8]. The innovation comes from the incorporation of tungsten (W) and boron (B) which allows respectively improving creep properties and preserving a good ductility. In addition, densifying the materials by spark plasma sintering technique proved interesting to favour fine microstructures. This process is based on powder metallurgy and allows very fast processing cycles, by applying a pulsed current and a uniaxial pressure on the powder. By heating the powder in the α+β field above the α+β+γ/ α+β line transformation of the phase diagram, a fine near-lamellar microstructure is obtained [10-11]. Mechanical properties [11] exhibited a very good compromise between elongation at room temperature (A = 1.6 %, when most TiAl alloys have a ductility below 1 %) and creep resistance (above 4000 h at 700°C under 300 MPa). The present study investigates the LCF behaviour and performance of IRIS at high temperatures and attempts to understand the cyclic deformation mechanisms.

2 Experimental procedure

2.1 Alloy composition and microstructure

The alloy investigated is the IRIS alloy with a composition of Ti-Al_{48}-W_2-$B_{0.08}$ (at%). Disks of 100 mm in diameter and 18 mm thick were densified by SPS in the FCT HPD-125 machine of the ICB Dijon in France. Temperature ramp was 100°C/min, and dwell temperature was 1375°C during 10min. At 1200°C, the temperature ramp was reduced to 25°C/min to avoid excessive overshoot. For these experiments, different dwell temperatures have been tested, in order to obtain the desired microstructure on more than ¾ of the diameter of the disks. Temperature was measured by a pyrometer at the center of the sample, 10 mm above the surface. The target microstructure (Figure 1) is formed by small lamellar colonies (35 to 45 μm in diameter), surrounded by γ grains (5 to 10 μm width) containing β_0 precipitates. Cylindrical specimens for the fatigue tests were then machined from SPS disks as illustrated in Fig 2.

* Corresponding author: Soumaya.Naanani@cemes.fr

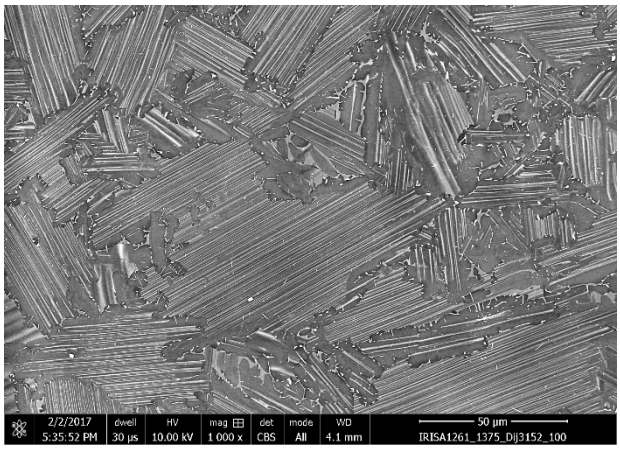

Fig.1. Near lamellar microstructure of the IRIS alloy densified by SPS.

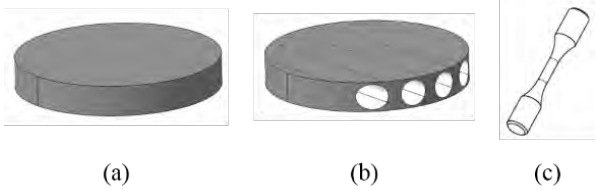

Fig. 2. (a) SPS disk of 100 mm in diameter and 15 mm in tickness of IRIS alloy with near lamellar microstructure. (b) Manufacturing of 4 cylinders per disk. (c) Machining of cylindrical fatigue specimen with: a gauge length of 14 mm, gauge diameter of 5 mm and a total length of 76 mm.

2.2 Low cycle fatigue test

Cylindrical specimen were mechanically polished in the gauge length with SiC papers in order to remove the surface irregularities due to the machining and minimise their effects on the fatigue life.
The low cycle fatigue tests were conducted on a MTS servohydraulic machine at a constant strain rate of 10^{-3} s^{-1} and at different total strain amplitudes ($\Delta\varepsilon_t/2$ = 0.3%, 0.45%, 0.6%) in symmetric tension compression cycle ($R_\varepsilon = \varepsilon_{min}/\varepsilon_{max} = -1$). The total strain amplitude was controlled by an extensometer directly placed on the gauge part of the specimens and which delivers a command signal adjusted in a triangular wave shape. All the tests were performed in air laboratory at three temperatures: 750, 800 and 850°C. Heating was ensured by an electrical resistance furnace providing a uniform temperature repartition on the specimen.

2.3 Fracture surfaces and microstructural observations

In order to identify and clarify failure mechanisms in IRIS, fracture surfaces were examined in a JEOL 2010 scanning electron microscope (SEM).
The cyclic deformed microstructures were analysed in a JEOL 2010 Transmission Electron Microscope (TEM) operating at 200 kV. Disks of 0.5 mm were cut perpendicularly to the tensile axis, close to the fracture surface and mechanically polished to a thickness of 20 µm and then electrolytically polished to electron transparency.

3 Results

3.1. Cyclic Stress Strain behaviour

Stress amplitudes as a function of the number of cycles at 800°C are presented for three different strain amplitudes in Fig.3. The cyclic behaviour is stable and no continuous hardening or softening is noticed. The fatigue life decreases as the total strain amplitude increases: from 5276 cycles for the lowest strain amplitude (0.3%) to 187 cycles for the highest strain amplitude (0.6%).

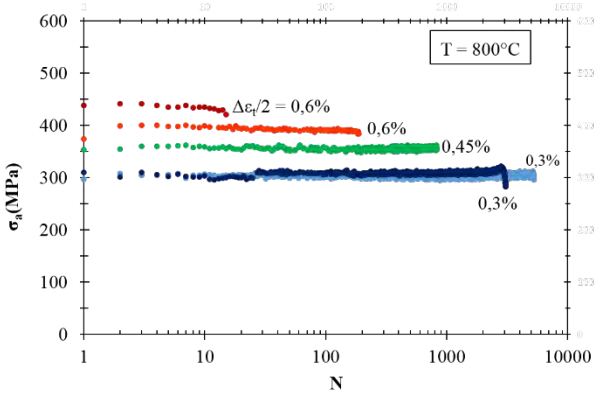

Fig.3. Stress amplitude versus number of cycles of IRIS alloy at 800°C.

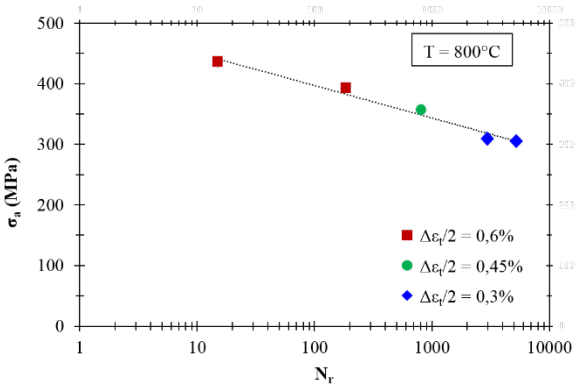

Fig.4. Stress amplitude versus number of cycles to failure for IRIS at 800°C.

An apparent dispersion of the number of cycles to failure for a given total strain amplitude is noticed (at $\Delta\varepsilon_t/2$ = 0.6% , N_f =15 and 187 cycles and at $\Delta\varepsilon_t/2$ = 0.3% , N_f = 5276 and 3071 cycles). However when plotting the stress amplitudes versus the number of cycles to failure for each fatigue test (Fig.4) all the results are on the same line. This indicates that the results are consistent and that fatigue life of IRIS can be easily predicted.

Tests at different temperatures were also performed to study the influence of the temperature on the fatigue life and the cyclic behaviour. Fig.5 shows stress amplitudes as a function of the number of cycles for the same total strain amplitude ($\Delta\varepsilon_t/2$ = 0.45%) at three different

temperatures: 750°C, 800°C and 850°C.

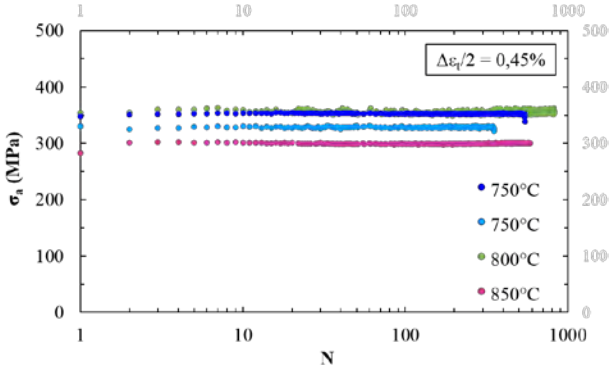

Fig.5. Stress amplitude versus number of cycles of IRIS alloy at high temperatures.

Cyclic behaviour is stable whatever the temperature. However, the fatigue life is lower at 750 and 850°C than at 800°C. This could be related to the brittle-ductile transition temperature, which occurs for this alloy between 700°C and 850°C as evidenced by Voisin et.al [11].

As specified in the introduction, literature provides many studies on LCF of TiAl alloys at various high temperatures and with various test conditions. It is thus difficult to strictly compare IRIS LCF behaviour with other TiAl alloys. However, focusing on a given temperature test, Table 1 presents some literature results of lamellar or near-lamellar TiAl alloys, obtained at 800°C with similar other test conditions (speed rates, strain amplitude).
Even if the microstructures and the speed rate of the LCF tests are not strictly the same, these results suggest that IRIS has higher fatigue lives than the TiAl alloys containing Nb at 800°C for the imposed strain amplitudes that has been investigated.

3.2. Fractures surface observations

All the fractures surfaces observations indicate a brittle fracture, typical of TiAl alloys [4]. Due to exposure of the fracture surfaces to air, an oxide layer has been formed (Fig.6).
For most of the fracture surfaces observed by optical and scanning electron microscope, the crack initiation site as well as the crack propagation regions are difficult to determine due to the rough surface and the absence of river patterns indicating the fatigue crack direction. The fracture surfaces analysed by SEM present a similar topography and the same fractures modes, regardless of the total strain amplitude applied. It consisted in a mixed mode comprising interlamellar and translamellar modes. These two modes are represented respectively by yellow and white arrows on figure 6. Secondary cracks along the lamellar colonies boundaries and interlamellar decohesion were also found (fig.7(a)). These fracture modes are typical of the TiAl alloys with lamellar microstructure [6][13-15].

However, the γ borders, which are important for the ductility of the alloy [11] are difficult to investigate: their size (5 to 10 μm width) and the irregular surface do not allow to detect their specific fracture mode.

3.3. Deformation mechanisms

The changes in the microstructure after fatigue failure were studied in specimens cycled at 800°C and for the extremes total strain amplitudes applied: 0.3% and 0.6%. In both specimens, the microscopic mechanisms have been investigated in the γ borders rather than in the lamellar colonies. The identification of the mechanisms is indeed more difficult in the latter case, due to perturbation of the dislocation morphologies by the lamellar interfaces. Globally, the presence of loops, twins, ordinary dislocations and debris are common to the two samples, but in a much higher proportion in the microstructure tested at 0.3%, as illustrated on figure 8. The microscopic mechanisms in the two samples are discussed in more details in what follows.

plane, represented in the stereographic projection (figure

Table 1. LCF results on TiAl alloys at 800°C

Composition (at%)	Microstructure	$\dot{\varepsilon}$ (s^{-1})	$\Delta\varepsilon_t/2$ (%)	σ_a (MPa)	N_f
IRIS : Ti-Al_{48}-W_2-$B_{0.08}$	Near-lamellar	10^{-3}	0.3	304 ; 310	5276 ; 3071
			0.45	356	828
			0.6	392 ; 435	187 ; 15
Ti-Al_{46}-NB_2-Cr_2 [6]	Near-lamellar	2.10^{-3}	0.35	290	1046
	Full-lamellar	2.10^{-3}	0.35	300	1238
			0.45	340	205
TiAl-8%Nb [15]	Lamellar	2.10^{-3}	0.3	350	1500
			0.42	410	120

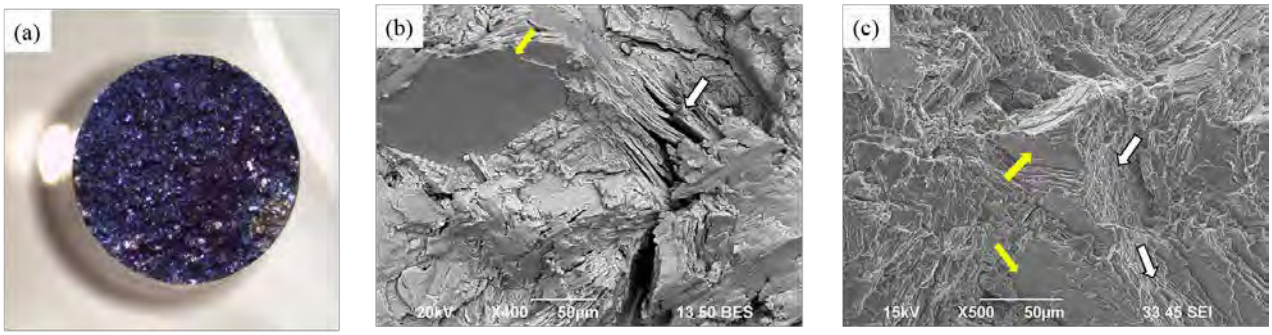

$\Delta\varepsilon_t/2$ = 0,6% ; N_f=187 cycles $\Delta\varepsilon_t/2$ = 0,6% ; N_f=187 cycles $\Delta\varepsilon_t/2$ = 0,3% ; N_f=3071 cycles

Fig.6. Fatigue fracture of specimens tested at 800°C. (a) General view (b) and (c) Yellow and white arrows indicates interlamellar and translamellar fracture respectively.

3.3.1 Deformation mechanisms in specimen: $\Delta\varepsilon_t/2$ = 0,6%; N_f =15 cycles

Figure 9 shows the activated deformation mechanisms in the γ borders cycled at high strain amplitude. The microstructure is mostly deformed by ordinary dislocations ($\vec{b}$ = 1/2 [$\bar{1}$10]) parallel to their screw direction (Figure 9. (a), (b)). These dislocations can be anchored at many pining points (Figure 9. (d)). Twinning is also observed in this specimen (Figure 9. (c)), but less commonly.

To identify moving planes of ordinary dislocations, tilt experiments were performed on several loops in the γ microstructure of this specimen. An example of these experiments is shown in figure 10. It consists in measuring the apparent width of the loop portion, at different inclination angles (represented respectively by W and θ in figure 10(b)). The variation of W according to θ corresponds to a sine curve (figure 10(c)), whose maximum (≈-18° in this case) represents the largest width of the portion loop. This identifies the moving 10. (b)) as a dotted line, and whose pole is marked as P. It can be seen that the moving plane is away of the Burgers vector $\vec{b}$ by only a few degrees, which is in the experimental errors of tilt experiments (±10°). Thus, it can be considered that P contains the loop, which indicates a glide mechanism.

Moreover, the plane P appears to be neither a common gliding plane one of the two possible (111) pure glide planes containing $\vec{b}$. So, the deformation mode activated here is cross slip. This procedure has been repeated for other ordinary loops and the deformation mechanisms found were either pure glide or cross glide.

3.3.2 Deformation mechanisms in specimen: $\Delta\varepsilon_t/2$ = 0,3%; N_f =5276 cycles

The same study was made on the specimen cycled at 0,3%. Dislocations density does not allow to perform many tilt experiments, it is indeed more difficult to find isolated loops. The microstructure revealed, as indicated above, a higher dislocation density than in the sample tested at $\Delta\varepsilon_t/2$ = 0.6%.

Figure 11 shows characteristic landscapes of deformed γ phase. γ borders can be deformed by ordinary dislocations ($\vec{b}_A$= 1/2 [$\bar{1}$10] and $\vec{b}_B$= 1/2 [110]) aligned in their Burgers vector (figure 11.(a)). However, unlike

* Corresponding author: Soumaya.Naanani@cemes.fr

the previous case ($\Delta\varepsilon_t/2$ = 0.3%), this is not the most frequent deformation mechanism.
The presence of twins is more important in this case (Figure 11(b) and (c)) and loops and debris are also present in a much higher proportion.

Figure 12 shows a tilt experiment of a loop identified as an ordinary dislocation ($\vec{b}=1/2[\bar{1}\bar{1}0]$). The stereographic projection shows that its Burgers vector does not lie in the loop plane (represented by a dotted line whose pole is marked as P on figure 12 (c)), this is therefore not a glide loop.

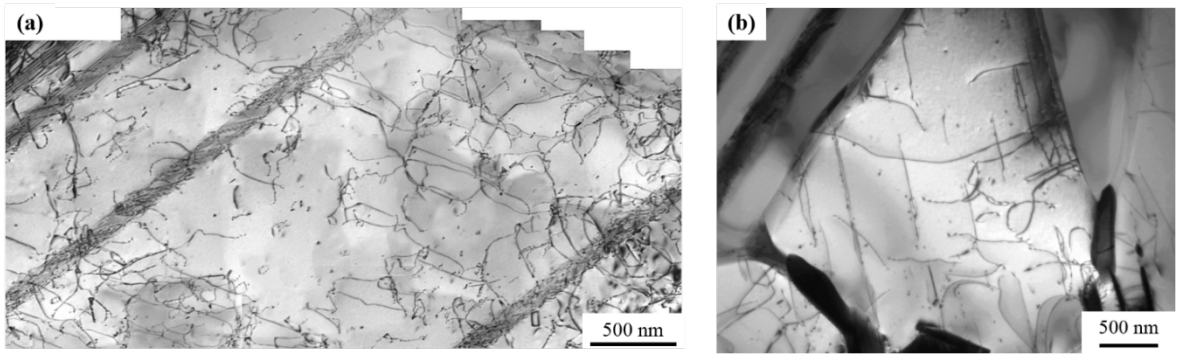

Fig.7. TEM observations of deformed microstructure at 800°C after fatigue failure in γ borders: (a) $\Delta\varepsilon_t/2$= 0,3%, N_f = 5276 cycles (b) $\Delta\varepsilon_t/2$= 0,6%, N_f = 15cycles

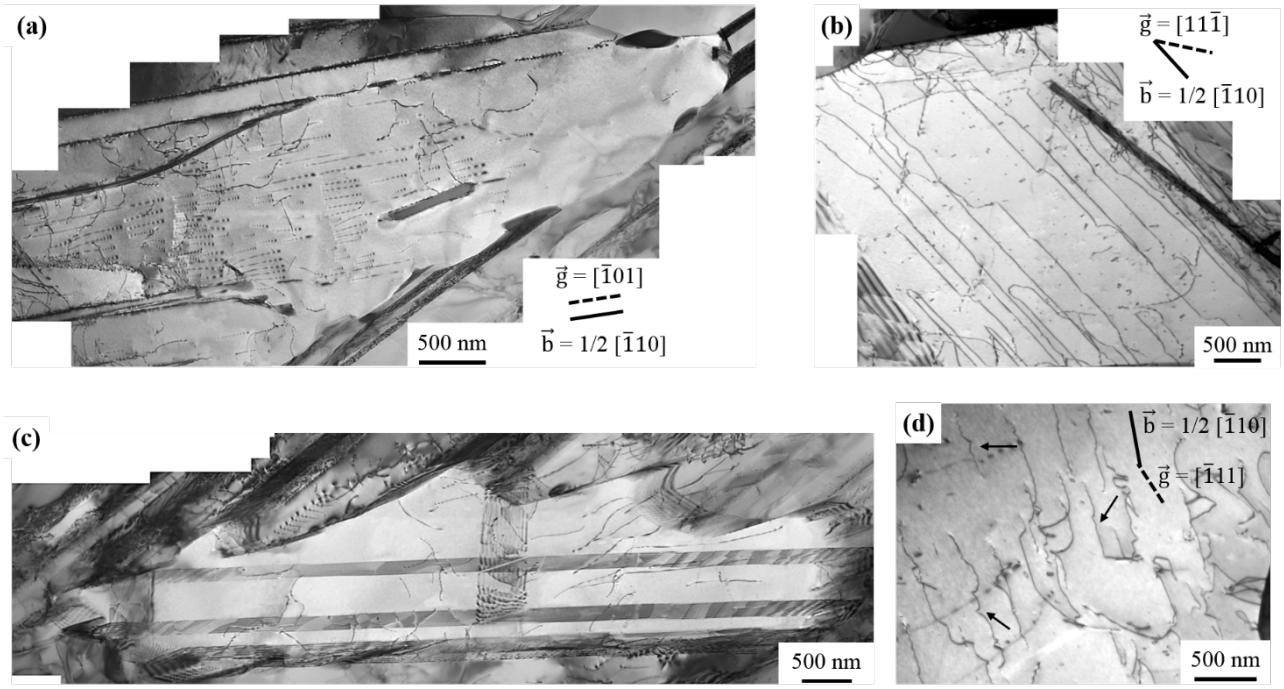

Fig.8. Deformation microstructure of γ grains for $\Delta\varepsilon_t/2$=0.6%, N_f = 15cycles, 800°C: (a) and (b) ordinary dislocations aligned in the screw direction. (c) Twins. (d) Pinning points

However this plane does not correspond to the pure climb plane [$\bar{2}\bar{2}$0] (represented in green on figure 12(c)), so the movement involved here is mixed climb.

Another tilt experiment on this microstructure indicated the presence of cross slip.

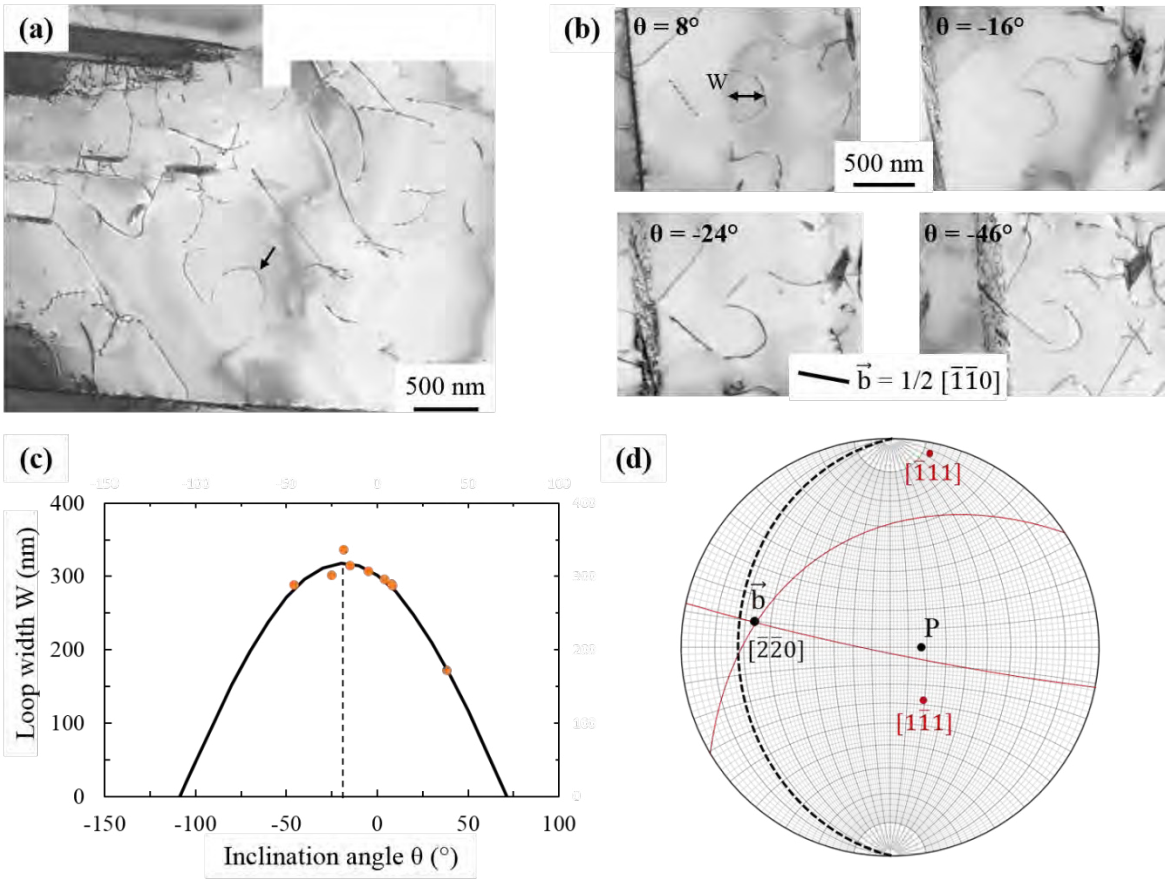

Fig.9. Tilt experiment on a loop portion in the sample tested at $\Delta\varepsilon_t/2 = 0.6\%$ ($N_f = 15$cycles). (a) General view of the γ grain that contains the loop. (b) Loop at different inclinations θ. (c) Variation of the loop width W according to the inclination angle θ. (d) Stereographic projection indicating the moving plane (dotted line), its pole (P), and two (111) planes (red lines).

* Corresponding author: Soumaya.Naanani@cemes.fr

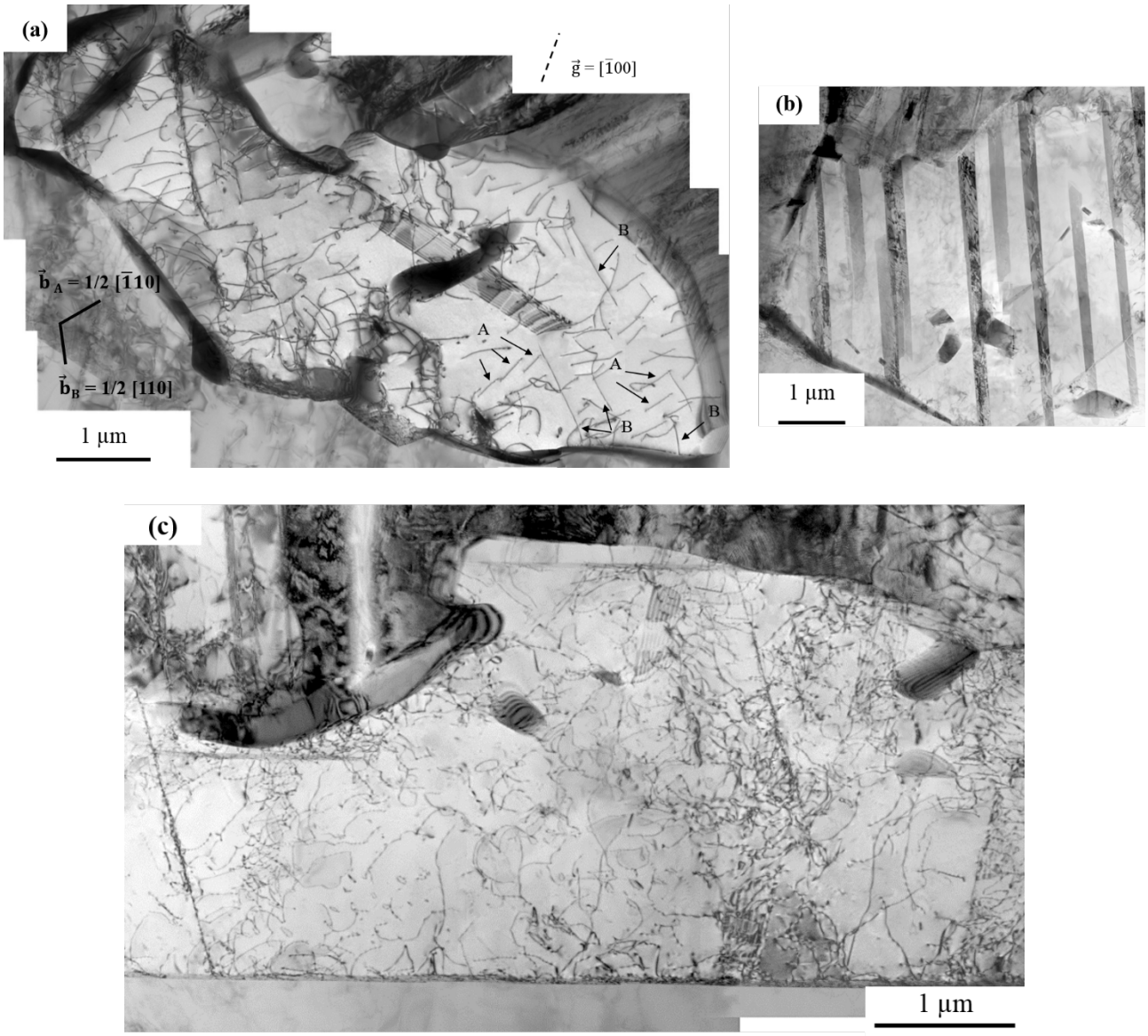

Fig.10. Deformed γ grains for $\Delta\varepsilon_t/2 = 0.3\%$ ($N_f = 5276$ cycles, 800°C): (a) ordinary dislocations, (b) twins, (c) loops, twins, debris and ordinary dislocations.

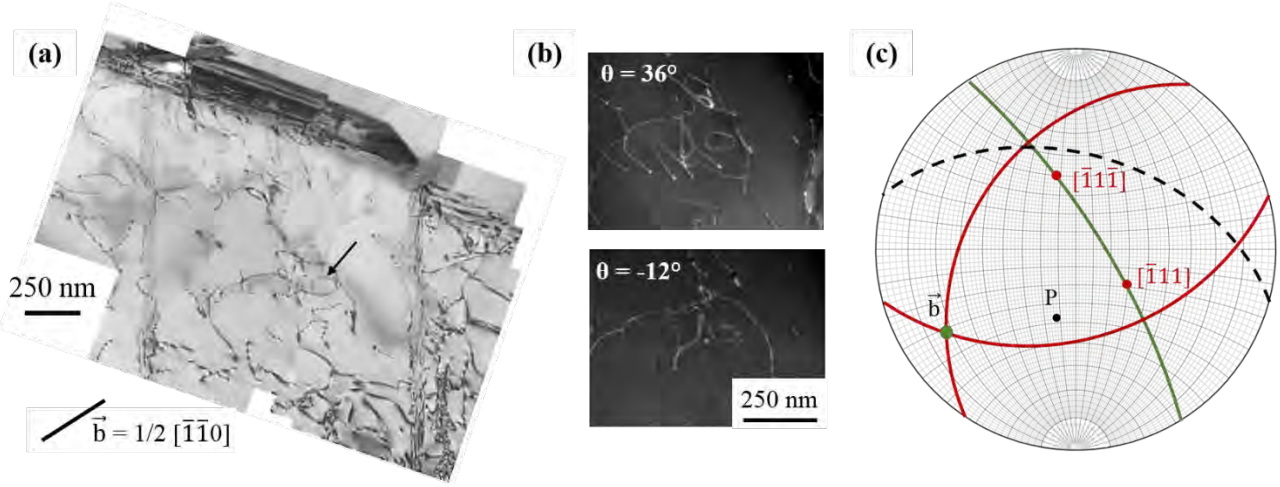

Fig.11. Tilt experiment on a loop portion in a γ grain of a sample tested at $\Delta\varepsilon_t/2 = 0.3\%$ ($N_f = 5276$cycles). (a) General view. (b) Loop at two inclinations θ. (d) Stereographic projection indicating the moving plane (dotted line), its pole (P), and two (111) planes (red lines)

4 Discussion

First results of investigation on LCF behaviour of IRIS at high temperatures (750, 800 and 850°C) are presented in this paper. The literature provides many fatigue tests results of TiAl alloys that are difficult to compare due to the various test conditions. When considering the few data available at 800°C with similar strain rates and strain amplitudes [6] [15], it appears that IRIS has a comparatively good lifetime.
Moreover the cyclic behaviour is very stable and no hardening or softening has been observed at the three temperatures. This feature is interesting in view of industrial use of the alloy, for which stable mechanical properties is an asset. The TiAl alloys with 2%Nb have a similar behaviour [6] [16] whereas TiAl-8%Nb present a noticeable softening at high temperatures [17] [15].

Temperature dependence appears rather weak, with only slight lifetime increase and decrease between 750°C-800°C, and between 800°C-850°C, respectively. This could be related to the brittle-ductile transition, which occurs around 800°C for this alloy [11]. Dependence on the imposed total strain amplitude follows a regular trend, indicating no abrupt change in damage mechanism.
Fracture follows a mixed interlamellar and translamellar propagation mode, which is usual in TiAl.

Study of the deformed microstructure at 800°C by TEM shows that the presence of ordinary dislocations, twins and loops are common to the two samples analysed. However, deformation at $\Delta\varepsilon_t/2 = 0.6\%$ is mainly controlled by glide of ordinary screw dislocations whereas at $\Delta\varepsilon_t/2 = 0.3\%$ there is no main deformation mechanism, several types of dislocations randomly organized are present. Unlike Sastry and Lipsitt [1], no braid structure has been observed.
TEM observations exhibit also that dislocation density is more important in the specimen deformed at $\Delta\varepsilon_t/2 = 0.3\%$ (N_f=5276 cycles and σ_a=304 MPa) than at $\Delta\varepsilon_t/2 = 0.6\%$ (N_f=15 cycles and σ_a=435 MPa). Density dislocation depends then on fatigue lifetime rather than on stress amplitude. This could be quantified by cumulative plastic strain ε_{pc} which corresponds to the sum of plastic strain of each cycle, and represents the forth and back movement of dislocations during the test. Table 2 shows that there is an important difference of this parameter between the two specimens: ε_{pc} is markedly more important for the specimens tested at $\Delta\varepsilon_t/2 = 0.3$ % (ε_{pc} = 491%) than at $\Delta\varepsilon_t/2 = 0.6$ % (ε_{pc} = 9%). The fact that the material can endure cumulated plastic strain as high as 491%, indicates clearly that most of the dislocation displacements are reversible during the tension and compression steps of the fatigue cycles, if not the specimen would be extremely deformed.

Table 2. Cumulative plastic strain ε_{pc} (%) of two specimen tested at 800°C.

$\Delta\varepsilon_t/2$(%)	σ_a (MPa)	N_f (cycles)	ε_{pc} (%)
0,3	310 MPa	3071	491
0,6	435 MPa	15	9

Furthermore during their reversible forth and back movement, the dislocations leave prismatic loops and debris, as observed in figures 9(b) and 11(c). However, all the movements are not completely reversible, and an increase in dislocation density occurs up to fracture. The high density of twins observed is compatible with reversibility of the motion of twins in tension and compression. Thus, the presence of twins probably explains also the rather low density of ordinary dislocations (lower than the density of dislocations which would be observed in samples deformed of 491%, without reversibility or recovery processes), most of the reversible deformation of the sample being accommodated by twinning. Finally, a high number of loops is observed. If they would be glide loops, they would very quickly annihilate due to very high line tension coming from their small diameter. Thus, they can only be prismatic and result from cross-slip processes [18]. At high temperatures, these loops would tend to vanish by climb mechanisms. Then, their stability is an approximate measure of the climb kinetics. In the study of Gloanec et.al [4], in situ TEM observations show that it takes about 25 minutes at 750°C for these loops to disappear. This shows that climb mechanisms are very slow in this temperature range, in reason of slow diffusion kinetics. The study of Kad and Fraser [19] shows that temperatures of 900°C are required to activate diffusion-controlled mechanisms for strain rates between 10^{-3} and 10^{-5} s^{-1}. However, some mixed-climb loops can form in the $\Delta\varepsilon_t/2 = 0{,}3\%$ experiments, as observed in Fig. 12. In this case, the duration of the experiments (18h) is high enough to allow growth of mixed-climb loops by diffusion processes. The contribution of this phenomenon to the total deformation, nevertheless, is believed to be negligible. Then, climb mechanisms are rather improbable in our experiments.

5 Conclusion

In this study, the IRIS alloy has been tested in low cycle fatigue, for temperatures ranges of 750-850°C and for total strain amplitudes $\Delta\varepsilon_t/2$ between 0.3 % and 0.6 %. The mechanical results and the microstructure characterizations by TEM lead to the following conclusions:

- The stress amplitude is remarkably constant during the tests, and the dependence of fatigue life on the strain amplitude follows a regular trend. Moreover, only weak temperature dependence is observed. These mechanical

* Corresponding author: Soumaya.Naanani@cemes.fr

properties are interesting in comparison with other alloys.

• Regular mixed interlamellar and translamellar propagation modes are observed, as usual in lamellar TiAl alloys.

• Dislocation density depends on fatigue lifetime rather than on stress amplitude.

• Deformation occurs mainly by ordinary dislocations and twins. The dislocation movements are found to be mainly reversible during the tension and compression steps, indeed extremely high dislocation densities are not observed, despite very elevated cumulative plastic strains (up to 491 %). Tilt experiments show slip and cross-slip are the preferred motion modes, climb being rather improbable.

This study has been conducted in the framework of the cooperative project "ALTIAERO" project of the "IDEX-ATS" program supported by the Université Fédérale – Toulouse Midi-Pyrénées, which is acknowledged.

References

1. S. M. . Sastry and H. . Lipsitt, Metall. Mater. Trans. A Phys. Metall. Mater. Sci., **8A**, 299–308, (1977).
2. H. Y. Yasuda, T. Nakano, and Y. Umakoshi, Philos. Mag. A, **71**, 127–138, (1995).
3. Y. Umakoshi, H. Y. Yasuda, and T. Nakano, Mater. Sci. Eng. A,**192–193**, no. PART 1, 511–517, (1995).
4. A. L. Gloanec, M. Jouiad, D. Bertheau, M. Grange, and G. Hénaff, Intermetallics, **15**, 520–531, (2007).
5. A. L. Gloanec, G. Henaff, M. Jouiad, D. Bertheau, P. Belaygue, and M. Grange, Scr. Mater., **52**, 107–111, (2005).
6. G. Malakondaiah and T. Nicholas, "High-temperature low-cycle fatigue of a gamma titanium aluminide alloy Ti-46Al-2Nb-2Cr," Metall. Mater. Trans. A, **27**, 2239–2251, (1996).
7. M. Petrenec, M. Šmíd, T. Kruml, K. Obrtlík, and J. Polák, "Low Cycle Fatigue of Cast γ-TiAl Based Alloys at High Temperature," Key Eng. Mater., **452–453**, 421–424, (2010).
8. T. Voisin, J. P. Monchoux, L. Durand, N. Karnatak, M. Thomas, and A. Couret, Adv. Eng. Mater., **17**, 1408–1413, (2015).
9. A. Couret, J. P. Monchoux, M. Thomas, and T. Voisin, "Procédé de fabrication d'une pièce en alliage en titane-aluminium," Patent WO2014199082 A1, (2013)
10. T. Voisin, J.-P. Monchoux, M. Perrut, and A. Couret, Intermetallics, **71**, 88–97, (2016).
11. T. Voisin, J. P. Monchoux, M. Thomas, C. Deshayes, and A. Couret, Metall. Mater. Trans. A Phys. Metall. Mater. Sci., **47**, 6097–6108, (2016).
12. K. S. Chan and D. S. Shih, Metall. Mater. Trans. A, **28**, 79–90, (1997).
13. B. D. Worth, J. M. Larsen, S. J. Balsone, and J. W. Jones, Mater. Trans. A**, 28**, (1997).
14. S. J. Balsone, B. D. Worth, J. M. Larsen, J. W. Jones, M. Directorate, and A. Arbor, Scr. Mater, **32**, 1653–1658, (1995).
15. T. Kruml and K. Obrtlík, Int. J. Fatigue, **65**, 28–32, (2014).
16. F. O. R. Fischer, H. J. Maier, and H. Christ, *Influence of Environment , Mean Stress and Temperature on the Low-Cycle Fatigue Behaviour of a Near- γ Titanium Aluminide*, (2000).
17. F. Appel, T. K. Heckel, and H. J. Christ, Int. J. Fatigue, **32**, 792–798, (2010).
18. D. Caillard, M. Legros, and A. Couret, Philos. Mag., **93**, 203–221, (2013).
19. B. K. Kad and H. L. Fraser, Philos. Mag. A Phys. Condens. Matter, Struct. Defects Mech. Prop., **69**, 689–699, (1994).